Density functional theory and molecular dynamics studies of the energetics and kinetics of electroactive polymers: PVDF and P(VDF-TrFE)

Haibin Su, Alejandro Strachan,* and William A. Goddard III[†]

Materials and Process Simulation Center, Beckman Institute (139-74), California Institute of Technology, Pasadena, California 91125, USA

We used first principles methods to study static and dynamical mechanical properties of the ferroelectric polymer poly(vinylidene fluoride) (PVDF) and its copolymer with trifluoro ethylene (TrFE). We use density functional theory [within the generalized gradient approximation (DFT-GGA)] to calculate structure and energetics for various crystalline phases for PVDF and P(VDF-TrFE). We find that the lowest energy phase for PVDF is a nonpolar crystal with a combination of trans (T) and gauche (G) bonds; in the case of the copolymer the role of the extra (bulkier) F atoms is to stabilize T bonds. This leads to the higher crystallinity and piezoelectricity observed experimentally. Using the MSXX first principles-based force field (FF) with molecular dynamics (MD), we find that the energy barrier necessary to nucleate a kink (gauche pairs separated by trans bonds) in an all-T crystal is much lower (14.9 kcal/mol) in P(VDF-TrFE) copolymer than in PVDF (24.8 kcal/mol). This correlates with the observation that the polar phase of the copolymer exhibits a solid-solid transition to a nonpolar phase under heating while PVDF directly melts. We also studied the mobility of an interface between polar and nonpolar phases under uniaxial stress; we find a lower threshold stress and a higher mobility in the copolymer as compared with PVDF. Finally, considering plastic deformation under applied shear, we find that the chains for P(VDF-TrFE) have a very low resistance to sliding, particularly along the chain direction. The atomistic characterization of these "unit mechanisms" provides essential input to mesoscopic or macroscopic models of electro-active polymers.

I. INTRODUCTION

Poly(vinylidene fluoride) (PVDF) and its copolymers with trifluoro ethylene (TrFE) exhibit excellent electro-mechanical properties such as ferroelectricity, piezoelectricity, pyroelectricity, and nonlinear optical properties.[1] Ferroelectricity in PVDF and P(VDF-TrFE) random copolymers was demonstrated with various experimental techniques [including x-rays, IR, polarization-field hysteresis loops, and the existence of a Curie point (only in copolymers)] in the late 1970s and early 1980s.[2] Very recently, Zhang and collaborators[3] showed that it is possible to make use of electric field-induced phase transformations between polar and nonpolar phases in nanostructured (via electron irradiation) P(VDF-TrFE) to obtain large electrostrictive strains (∼5%) at high frequencies (1000 KHz) and with good energy densities (comparable to the best piezoceramics). Such materials are very attractive for many applications requiring soft transducers, due to good acoustic impedance match with biological tissue and water.

Molecular dynamics (MD) have previously been used to study electromechanical properties of PVDF[4,5] and P(VDF-TrFE)[6–11] including the prediction of elastic, dielectric, and piezoelectric constants, and polar to nonpolar phase transition. However, despite experimental and theoretical efforts and the technological importance of this class of materials, the fundamental molecular processes responsible for their macroscopic electromechanical properties are largely unknown. A quantitative characterization of such processes is necessary to build predictive, first principles-based materials models and should be helpful for the design of materials

with improved properties (such as actuators with higher strain, precision, frequency, and energy density).

In this paper we use atomistic modeling [DFT and first principles-based force fields (FFs) with molecular dynamics (MD)] (described in Sec. II) to study (i) structures and energies of various crystal structures (Sec. III); (ii) the nucleation energy associated with the polar to nonpolar phase transformation and phase boundary propagation as a function of applied external stress (Sec. IV); and (iii) chain sliding under shear deformation (Sec. V). Finally, conclusions are drawn in Sec. VI. The comparison between the behavior of PVDF and P(VDF-TrFE) random copolymers allow us to quantify the effect of the trifluoro ethylene (TrFE) segments on various materials properties.

A. Crystal structures of PVDF

Four crystalline polymorphs of PVDF are well characterized experimentally; they are generally referred to as I, II, III, and IV. Following Ref. 4 we refer to these as follows: I=T_p, II=TG_{ad}, III=T_3G_{pu}, and IV=TG_{pd} (see Fig. 1). In this notation we indicate the chain conformation with capital letters (T means all-T, TG means TGTG′, and T_3G indicates TTTGTTTG′) the subscripts p or a indicate polar phases with parallel dipoles and nonpolar phases with antiparallel dipole moments, respectively; finally the subscripts u and d indicate up-up or up-down relative directions of adjacent chains.[4] When PVDF is cooled from the melt, the TG_{ad} phase is obtained. The polymer chains contain T and G bonds in a TGTG′ sequence. This phase has a polar counterpart: the TG_{pd} phase. The main difference between them is the orien-
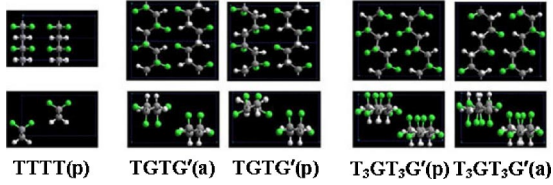
FIG. 1. (Color online) Crystal structures of various phases for PVDF. The polar phases with parallel dipole moments are denoted by (p), while nonpolar phases with antiparallel dipole moments are denoted by (a). The existence of the nonpolar T_3G_{ad} phase was conjectured by Lovinger[12] and proved by Karasawa and Goddard.[4]

tation of the dipole moments. In TG_{pd} they are parallel while in TG_{ad} they are antiparallel. The TG_{ad} phase can be converted into TG_{pd} simply by poling with an electric field of ~100 MV/m. If TG_{ad} phase is annealed at high temperature, the polar T_3G_{pu} phase is formed with a TTTGTTTG′ conformation. In analogy to the TG phases, there might exist a nonpolar T_3G_{au} phase as suggested by Lovinger[12] and confirmed by simulations.[4] In fact, we will use this phase to model the nonpolar phase with T_3G conformation observed experimentally[3] in electron irradiated P(VDF-TrFE). The most interesting polymorph for ferroelectricity is phase T_p; it can be obtained by mechanical drawing from T_3G_{pu} phase or poling from TG_{pd} with a ~500 MV/m electric field. The polymer chains are in an all-T configuration and packed in a parallel fashion.

Changes in molecular conformation (T, TG, T_3G) lead to significant shape changes. As shown in Fig. 1 the all-T crystal is longer along the chain direction and shorter in the directions perpendicular to it than TG and T_3G phases. This type of structural change is quite different from that in the ceramic ferroelectric compounds in which small ionic groups change their dipole orientation by rotation and/or displacement. In the polymer system the dipoles are linked together by strong covalent bonds and so that orientational change in the dipole moments requires cooperative motion of neighboring groups through large-scale T-G conformational changes.

II. METHODS

The *ab initio* QM calculations in this paper were performed using the DFT pseudopotential code SeqQuest[13,14] which uses Gaussian basis sets. For all calculations (described in Sec. III) we used the Perdew, Burke, and Ernzerhof implementation of the generalized gradient approximation (GGA).[15] The SeqQuest code calculates atomic forces and the stress tensor which were used to relax positions and cell parameters.

The characterization of many important materials properties require the simulation of large systems (thousands of atoms) for relatively long times (nanoseconds) making QM methods impractical. Thus we use the first principles-based force field MSXX[4] with MD to study energetics, nucleation energies, interface mobility, and viscoelastic properties. The MSXX force field describes the atomic interactions with three energy terms: (i) electrostatic interactions using QM-derived charges; (ii) covalent interactions (bonds, angles, tor-

sions, and cross terms obtained using the Hessian biased method to fit QM vibrational frequencies; and (iii) van der Waals interactions parametrized to reproduce mechanical properties of polyethylene, graphite, CF_4 and poly(tetrafluoroethylene) crystals. In order to describe the TrFE segments we extended the MSXX FF by describing the fluorine atom in the CHF group as the F atoms in VDF (same atom type and charge), the corresponding carbon is treated as the CF_2 carbon in MSXX (denoted C_{3VF} as in Ref. 4) with its charge modified to maintain charge neutrality. New three- and four-body terms are calculated using combination rules. The supplementary material contains all the force field parameters.[16] This simple extension of the MSXX FF allows us to characterize the effects of the presence of TrFE and PVDF.

All the simulations in this work use periodic boundary conditions, with the z axis is oriented paralled to the polymer chain direction and they y axis in the direction of the polarization.

III. ENERGETICS OF VARIOUS CRYSTALLING PHASES: DFT-GGA AND MSXX FORCE FIELD

A key issue to understand the electromechanical properties of these polymers is the relative energies and structural changes among the various phases and the origins of such differences. We used DFT-GGA and the MSXX force field to study the relative energetics and structures of various crystalline phases $(T, TG_{ad}, TG_{pd}, T_3G_{pu}, T_3G_{au})$ for PVDF and P(VDF-TrFE) (50-50) copolymer (50 mole percent VDF). Table I summarizes the energetics calculated by optimizing atomic positions and cell parameters of various phases and isolated chains with periodic boundary conditions. Table I also gives lengths corresponding to four monomers of infinite (periodic) isolated single chains [in practical terms we performed these calculations using three dimensional periodic cells with large (50 Å) lattice parameters in the directions perpendicular to the chain direction and optimized the lattice parameter along the chain]. Here, the crystal cohesive energy (E_{coh}) is defined as

$$E_{coh} = E_{crystal} - N \times E_{isolated-chain}, \qquad (1)$$

where N is the number of chains inside the crystal phase, $E_{crystal}$ is the energy of the crystal phase, and $E_{isolated-chain}$ is the energy of corresponding (same chain conformation) isolated chain. All energies in Table I are given in kcal/mol per carbon atom. DFT-GGA predicts the TG conformation as the ground state for the isolated chains. Next, in relative stability (0.97 kcal/mol higher) is the T_3G conformation while the all-T chain has a much higher energy (1.41 kcal/mol higher than T_3G). We find that adding fluorine to make P(VDF-TrFE) leads to substantial stabilization of the all-T configuration. Although the TG conformation is still most stable (by 1.08 kcal/mol), the T_3G structure is higher in energy than all-T by 0.06 kcal/mol. Thus the extra F in the copolymer favors all-T conformations. The MSXX force field correctly describes the relative stability among different conformations in PVDF and the role of F in P(VDF-TrFE) (50-50), in ad-

TABLE I. Energetics of crystalline phases and isolated infinite chains of PVDF and P(VDF-TrFE) (50-50). All energies are given in kcal/mol per carbon atom. The reference energies for crystal phases and chains are the energy of T_p phase and all-T chain, respectively. The cohesive energy defined by Eq. (1) in the text is denoted by E_{coh}. The length (L) of isolated chain is defined as the length of four monomers along the chain direction. (QM) denotes DFT-GGA data; (FF) denotes MSXX force field.

Crystal	PVDF				P(VDF-TrFE)			
	ΔE (QM)	E_{coh} (QM)	ΔE (FF)	E_{coh} (FF)	ΔE (QM)	E_{coh} (QM)	ΔE (FF)	E_{coh} (FF)
T_p	0	−2.10	0	−3.98	0	−0.86	0	−3.02
TG_{ad}	−0.59	−0.31	0.39	−2.40	1.86	2.09	1.17	−0.72
TG_{pd}	−0.62	−0.34	0.35	−2.45	2.42	2.65	1.26	−0.62
T_3G_{pu}	−0.51	−1.20	0.19	−3.14	−0.17	−1.10	0.58	−2.49
T_3G_{au}	−0.38	−1.03	0.23	−3.10	−0.30	−1.23	0.56	−2.50
Single chains	ΔE (QM)	ΔE (FF)	L (Å) (QM)	L (Å) (FF)	ΔE (QM)	ΔE (FF)	L (Å) (QM)	L (Å) (FF)
T	0	0	5.22	5.13	0	0	5.19	5.21
TG	−2.38	−1.19	4.66	4.56	−1.08	−1.13	4.71	4.68
T_3G	−1.41	−0.65	4.62	4.54	0.06	0.05	4.72	4.70

dition to a good description of the lengths along the chain direction for various conformations.

In the case of condensed-phase PVDF, DFT-GGA yields a large stabilization of the all-T crystal structure with a cohesive energy of 2.10 kcal/mol per carbon, followed by T_3G phases ($E_{coh} \sim 1.1$ kcal/mol). Finally TG phases are less favored by crystallization with $E_{coh} \sim 0.3$ kcal/mol. This stabilization of T conformations due to better packing, represented by the difference in cohesive energies, is not enough to reverse the relative energetic stability of the phases: our calculations indicate that TG_{pd} phase is the most stable crystal followed by the TG_{ad} phase. The MSXX force field overestimates the cohesive energies, but exhibits trends from PVDF to copolymer in agreement with QM. This overestimation of E_{coh} leads to an incorrect ordering of the phases: MSXX predicts the all-T phase to be the most stable one. Adding F to make P(VDF-TrFE) (50-50) has the same effect as in the chains: it favors all T conformations. QM predicts the T_3G_{au} phase to be the ground state, followed by T_3G_{pu} (0.13 kcal/mol higher) and all-T (0.30 kcal/mol higher than T_3G_{au}). Again the effect of F is the favor T configurations; this could be an important factor in the better crystallinity (and consequently better piezoelectric properties) in the copolymer as compared with PVDF observed experimentally.[17]

Zhang et al.[3] observed experimentally a phase change from a polar all-T to nonpolar T_3G phase when P(VDF-TrFE) is irradiated with high-energy electrons. This treatment leads to a lower degree of crystallinity and consequently shorter coherence length of the crystalline regions; this may lead to an increase in the chain-chain separation distance. Our simulations explored two extreme cases of chain-chain separations: perfect crystals and isolated chains; our results are consistent with the observation in Zhang's experiments and quantify the effect of interchain cohesive energy.

IV. PHASE TRANSFORMATION: NUCLEATION AND PROPAGATION

Phase transitions can be induced in PVDF and its copolymer with TrFE by temperature, stress or an external electric field. Understanding the molecular level mechanisms responsible for these phase changes is important for manufacturing and processing[2] as well as to understand the excellent electromechanical properties of electron irradiated P(VDF-TrFE) samples.[18]

X-ray diffraction, Fourier transform infrared spectroscopy (FTIR), and differential scanning calorimetry have been used to characterize the microstructural changes induced by high energy electron irradiation in P(VDF-TrFE).[18] It was found that irradiation reduces the degree of crystallinity of the sample decreasing the size of the polar domains below a critical value where the crystalline regions transform to a nonpolar combination of T and G bonds (mainly formed by T_3G segments). This nanostructural change leads to a desirable decrease in polarization hysteresis; however for irradiation doses higher than the optimum (~ 75 Mrad) the hysteresis increases again.[18] This re-entrant hysteresis is believed to be caused by a high density of cross linking due to high irradiation doses.[18] The complex nanostructure resulting from irradiation shows excellent electromechanical properties such as $\sim 5\%$ electrostrictive strain resulting from an electric field induced, reversible phase transition between a nonpolar T_3G and the polar all-T crystal.[3,18,19] An atomistic simulation that fully captures the nanostructure of the irradiated copolymers would involve system sizes well beyond current capabilities. Thus in this section we characterize two "unit" mechanisms that play a key role in the properties of the irradiated copolymers and shed some light into phase transitions in PVDF and P(VDF-TrFE) in general.

Previous theoretical studies have focused on phase transitions in PVDF and its copolymers, including the thermal induced ferroelectric transition[9–11] and field induced TG_{ad}-TG_{pd} transitions.[20,21] These phase transitions are generally believed to occur via a nucleation and growth process,[2] governed by cooperative chain rotations and the motion of phase boundaries.[2]

Here we characterize (i) the nucleation of a kink (G bond pairs separated by T bonds) in a perfect T_p crystal; and (ii) the mobility of an interface between T_3G_{ad} and T_p phases
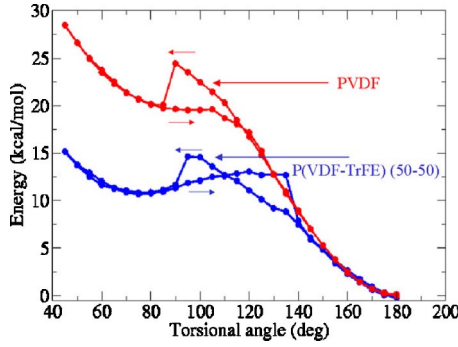
FIG. 2. (Color online) Energy barrier to nucleate a G bond in a T_p perfect crystal both PVDF and P(VDF-TrFE) (50-50). We used supercells consisting of 16 chains each consisting of eight mo-momers (2112 atoms).

[the phase transition believed to be responsible for the large electronstrictive strain in electron irradiated P(VDF-TrFE)].[19] We focus on the difference in behavior between PVDF and its 50-50 copolymer with TrFE.

A. Nucleation of a kink in an all-T configuration

In phase transitions originating from the all-T ferroelectric (I_p) phase [such as the ferroelectric-paraelectric (F-P PT)], the first unit process is the formation of gauche pairs separated by one or more trans bond (denoted as kinks). We use the MSXX FF to calculate the energy barrier and molecular level mechanisms associated with this process. To do this we start from a perfect T_p crystal and impose a harmonic restraint to one dihedral angle; we then minimize the total energy of the system (including the restraint) as the equilibrium angle of the restraint is changed from T to G in small steps (5°). For each restraint angle (θ_0) we fully relax the system including lattice parameters at zero applied stress. The PVDF simulation cell used for this calculation was built from the T_p unit cell (two monomers) replicating it 4 times in the x direction, 4 times in the y direction, and 20 times in the z direction. The resulting cell contains 16 infinite chains (40 monomers in each simulation cell per chain) and 1920 atoms. The copolymer was obtained from the PVDF cell by randomly converting 50% of the CH_2 groups into CHF.

Figure 2 shows the total energy as a function of θ_0 as the chosen torsion bond changes from T to G and back to T both for PVDF and P(VDF-TrFE) (50-50). For PVDF we obtain an energy barrier of 24.8 kcal/mol while for the copolymer the barrier reduces to 14.9 kcal/mol. Thus our simulations indicate that nucleation of the F-P PT takes place much easier in P(VDF-TrFE) than in PVDF. Experiments show that under heating PVDF in the T_P phase melts without a F-P PT, but in P(VDF-TrFE) the F-P PT is observed before melting for concentrations of TrFE larger than 18%. While the molecular level mechanism of the phase transition is not fully understood and defects (for instance the interface between crystalline and amorphous regions[21,22] can play a key role, our calculated nucleation barriers and the experimental results on phase transitions support nucleation and growth as the process responsible of the phase transition.
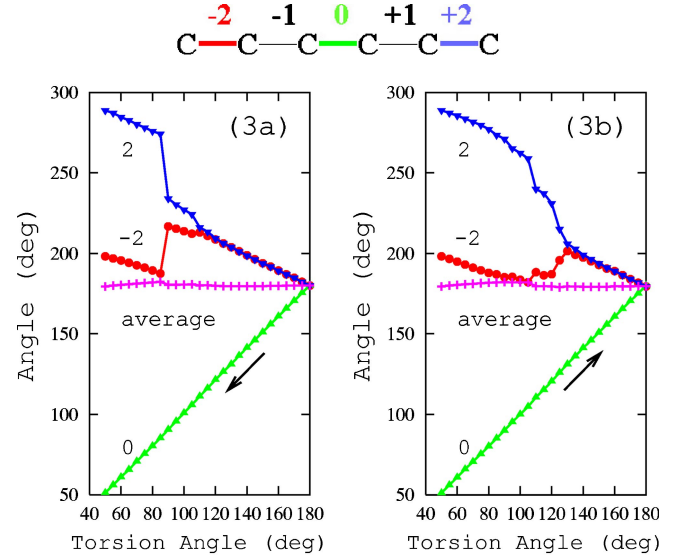

FIG. 3. (Color online) Evolution of various torsion angles in PVDF as a function of the restraint dihedral angle at its transform from T to G. The diagram at the top shows the notation: the restraint is applied to torsion angle for the bond denoted 0. We find that the first nearest neighbor bonds to the restraint one (+1 and −1) remain in the T conformation, while the second nearest neighbor bonds (+2 and −2) change to compensate for the changes in bond 0. The purple curve (pluses) shows that the average of the torsion angles remains at 180 degrees, which is topologically necessary since the chains are infinitely periodic. (a) corresponds to restraint varying from 180 to 50 while (b) reflects the reverse process.

Since the polymer chains are infinitely periodic (each chain is bonded to itself at the cell boundary) a T-to-G change in any one dihedral angle must be accompanied by compensating changes in the opposite direction in other bonds. To investigate this effect, we examined the change in dihedral angles for bonds neighboring the restrained one (denoted as 0) as a function of θ_0, see Fig. 3. We find that the angles centered around bonds that are first nearest neighbors to the restrained one (denoted ±1) remain T, no change during the process. This is because neighboring G bonds are quite unfavorable energetically. We find instead that it is torsions around the second nearest neighbor to the restraint bonds that completely compensates for the change in dihedral angle of bond 0. Thus as bond 0 transforms to G one of the second nearest neighbors goes to $\bar{G}$. The average between angles 0, −2, and 2 remains almost constant at the T value during the transformation (see magenta line in Fig. 3).

Finally, there is a correlation between the sudden energy drop seen in Fig. 2 and abrupt changes in the +2 and −2 dihedral angles. For small deformations starting from the all-T conformation the +2 and −2 angles counter the restraint in equal amounts (see Fig. 3). For $\theta_0 = 90°$ the angle −2 drops back to ∼180° and +2 doubles its contribution. This structural relaxation leads to a drop in the energy (see Fig. 2). A similar phenomenon occurs when the restraint angle is changed back to 180°.
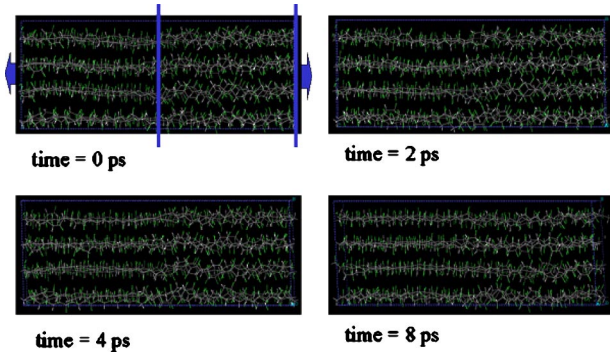
FIG. 4. (Color online) Snapshots of the $T_3G_{ad}-T_p$ interface for P(VDF-TrFE) (50-50) under 1.6 GPa tensile stress as various times obtained from the MD simulation.

B. Mobility of the interface between polar and nonpolar regions

We now turn to the second component in the nucleation and growth process: the velocity at which the already nucleated phase transition propagates; this is a critical property key to the performance of electron irradiated P(VDF-TrFE).

Fourier transform infrared spectroscopy shows that electron irradiation of P(VDF-TrFE) random copolymers decreases all-T content and increases T_3G segments;[18] an electric field-induced phase transition between these two phases is responsible for its electromechanical properties. Therefore, we model the irradiated material by a simulation cell containing nonpolar T_3G_{au} and all-T phases and studied the mobility of the interface between them them under tensile stress. The interface plane is perpendicular to the direction of the infinite chains (see Fig 4). The simulation cell contains 2112 atoms, 4 by 4 chains in the x and y directions with each chain containing 44 monomers in the periodic cell. We equilibrate the system using NPT MD simulations with the MSXX FF at $T=300$ K and zero stress. Using average lattice parameters obtained from the diagonal components of the shape matrix during the NPT run and 90° cell angles, we performed 40 ps of NVT simulations to further equilibrate our system. After this procedure residual stress was less than 0.05 GPa. The interface between all-T and T_3G phases did not move during the equilibration process (it is well known experimentally that drawing is necessary to obtain an all-T configuration). We then applied a tensile uniaxial stress along the chain direction using NPT dynamics; the stress was increased from zero at a loading rate of 0.5 GPa per ps until the desired stress was achieved, then the applied tensile stress was maintained and the interface mobility studied. Figure 4 shows snapshots of this process for P(VDF-TrFE) (50-50) with an applied stress of 1.6 GPa.

Figure 5 shows the percentage of T bonds in the system as a function of time for various applied stresses for PVDF [Fig. 5(a)] and P(VDF-TrFE) (50-50) [Fig. 5(b)]. Bonds are classified as T or G based on their dihedral angles. From the number of G bonds as a function of time we compute interface mobility, v, using the following equation:
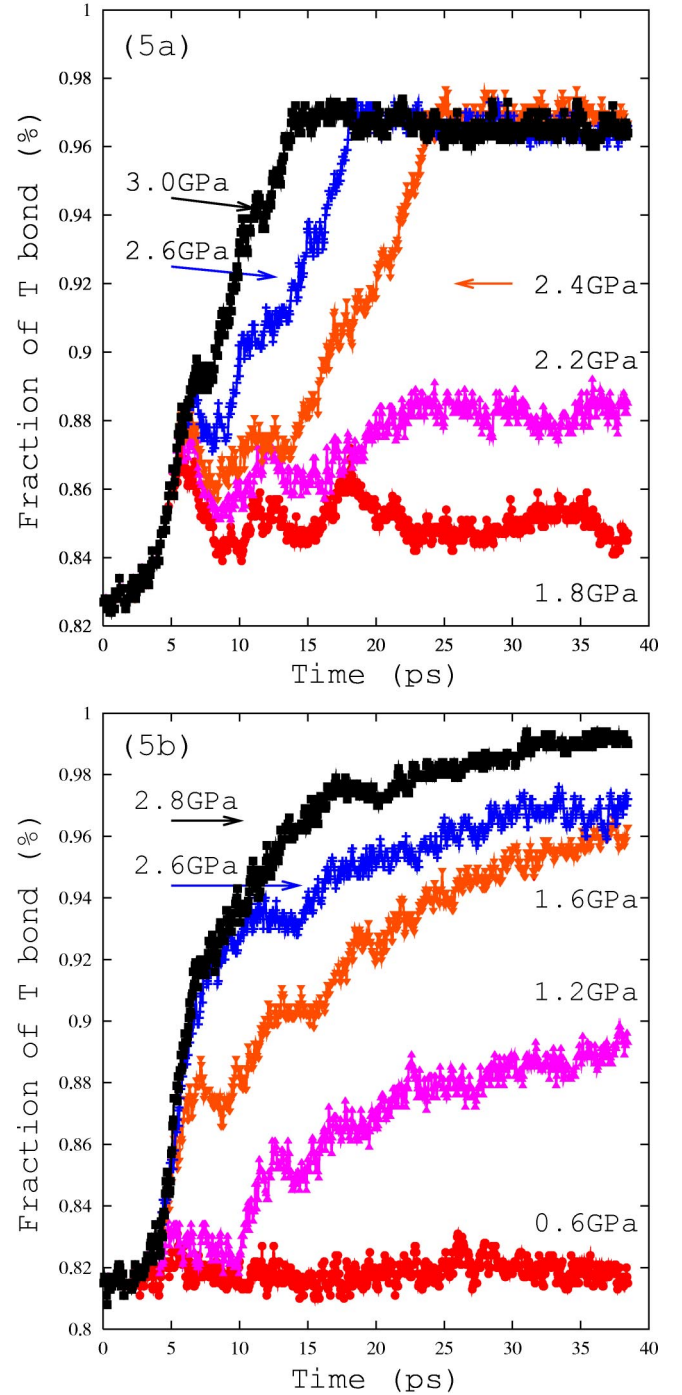

FIG. 5. (Color online) T_3G_{ad}-T_p interface mobility. Number of T bonds as a function of time for PVDF (a) and P(VDF-TrFE) (50-50) (b) under various uniaxial stress states at $T=300$ K.

$$v = \frac{\delta n \times L}{\delta t}, \qquad (2)$$

where δn is the change in the number of T bonds during the time period δt normalized to the number of chains in the simulation cell, and L is the length of the T_3G unit along chain direction. The calculated interface mobilities are plotted in Fig. 6. First, we notice that the threshold tensile stress
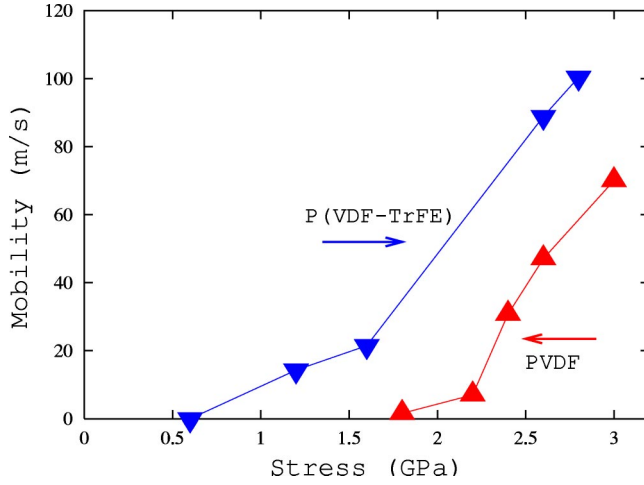
FIG. 6. (Color online) T_3G_{ad}-T_p interface mobility as a function of applied uniaxial stress for PVDF and P(VDF-TrFE) (50-50) at T=300 K.

to move the interface for P(VDF-TrFE) is about 1 GPa, while for PVDF it is much larger (~2 GPa). This explains why it is easier to draw nonpolar phases into polar phases in the case of the copolymer as compared with PVDF. Second, we find that the domain interface mobility is much larger in the case of the copolymer; for example, we find a velocity of 70 m/s for PVDF under a tensile stress of 3 GPa and 100 m/s for P(VDF-TrFE) under 2.8 GPa. These velocities are less than one-hundredth of the speed of sound propagating in PVDF and P(VDF-TrFE). [The sound velocity in the ⟨001⟩ direction is about 12 km/s and 11 km/s for PVDF and P(VDF-TrFE) T_p phases respectively.] We note that MD simulations incorporate in a natural way the many-body effects and cooperative phenomena involved in the motion of a domain boundary.

V. CHAIN SLIDING UNDER SHEAR DEFORMATION

The various crystalline structures of PVDF and P(VDF-TrFE) are formed by covalently bonded chains packed in a parallel fashion interacting via weak van der Waals forces. Since the various phases have large differences in length along the chain direction, we expect interchain slip to be an important mechanism during the phase transition, especially when the interface separating the two phases is along the chains. This process may play an important role to release deviatoric stresses that build up during phase transitions [as when electrostrictive P(VDF-TrFE) is used as an actuator].

Two popular methods for studying the viscous properties in molecular simulations are (i) the Green-Kubo (GK) method to analyze the time integral of the stress-stress correlation function during equilibrium molecular dynamics leading directly to the ordinary viscosity at zero strain rate,[23] and (ii) nonequilibrium molecular dynamics (NEMD) in which a deformation is imposed on the system and the time-averaged resulting component of the stress tensor is calculated; the stress-strain rate data can then be used to calculate viscosity as a function of strain rate. In this paper we use the
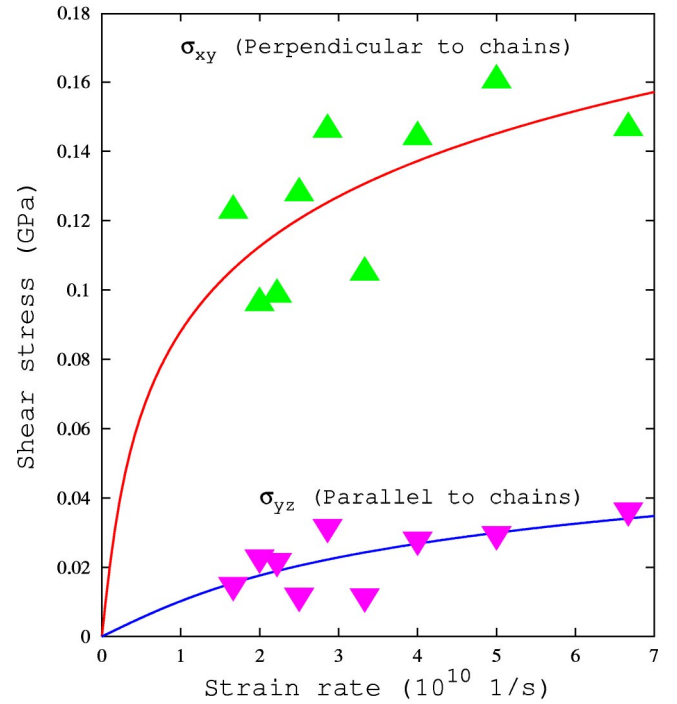

FIG. 7. (Color online) Shear stress and a function of applied strain rate for deformation in two different orientations with respect to the polymer chains for P(VDF-TrFE) (50-50) at 300 K. Lines represent fits to the MD data using the hyperbolic since function.

NEMD technique, imposing volume-conserving pure shear deformation to our simulation cells in two directions for various strain rates.

Using the convention that the c axis is the chain direction and the b axis is parallel to the dipole moments of the T_p phase, we deformed T_p P(VDF-TrFE) crystals along the following systems: (i) on the (100) plane in the ⟨010⟩ direction (denoted as perpendicular to the chains) and (ii) on the (010) plane in the ⟨001⟩ direction (denoted as along the chains). We applied strain rates in the range 1.66×10^{10} 1/s to 6.67×10^{10} 1/s using simulation cells containing $2 \times 4 \times 4$ unit cells (384 atoms). Symbols in Fig. 7 show the resulting averaged shear stress as a function of the imposed strain rate for both the perpendicular and parallel cases. We fitted our data to the widely used inverse hyperbolic sine flow equation:

$$\sigma(\dot{\gamma}) = \frac{k_B T}{V_0} \sinh^{-1}\left(\frac{\dot{\gamma}}{\dot{\gamma}_0}\right), \qquad (3)$$

where σ is the shear stress, $\dot{\gamma}$ is the strain rate, V_0 denotes the effective volume of the unit deformation, and $\dot{\gamma}_0$ is a characteristic frequency (inverse time). The fitted functions are shown as solid lines in Fig. 7. The flow equation [Eq. (3)] is very general in nature and can describe various mechanisms such as free volume-based deformation in metallic glasses[24,25] and dislocation-based single crystal plasticity.[26,27] The resulting effective volume in the parallel case is V_0 =281.4 Å^3 and in the perpendicular direction is 116.3 Å^3; the characteristic frequencies $\dot{\gamma}_0$ are 1.33×10^{10} 1/s and 0.17×10^{10} 1/s in the parallel and perpendicular directions, respectively. As expected, we find that the direction of easy
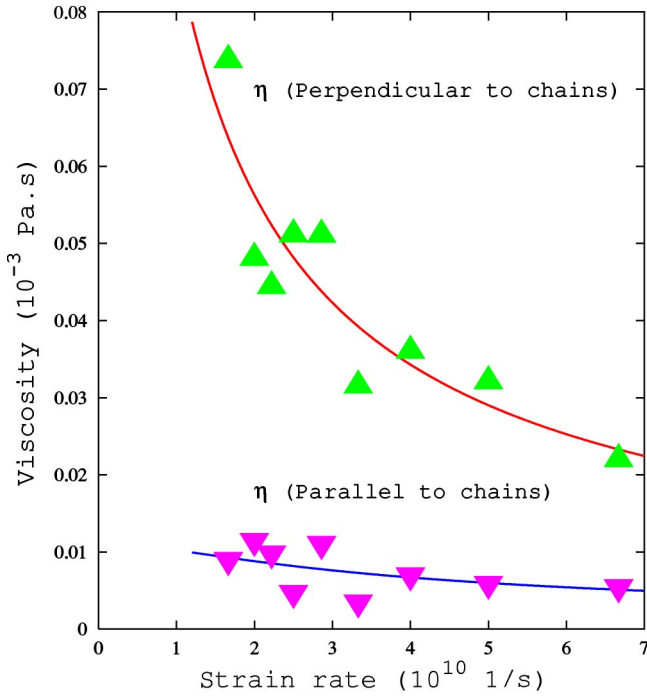
FIG. 8. (Color online) Viscosity for two different orientations with respect to the chains of P(VDF-TrFE) (50-50) at 300 K. Points represent MD data and lines were obtained from the fits to the stress-strain rate data using Eq. (3).

FIG. 9. (Color online) Snapshots obtained from MD simulation of shear deformation of a P(VDF-TrFE) (50-50) crystal using strain rate of 4.0×10^{10} 1/s in the direction parallel (a) and perpendicular (b) to the polymer chains.

slip has a larger characteristic frequency [$\dot{\gamma}_0$ is proportional to exp $(\Delta G / k_b T)$ where ΔG is an activation barrier[24–26]] and a larger effective volume.

We calculate viscosity (η) as $\eta = \sigma / \dot{\gamma}$; Fig. 8 shows the viscosity as a function of strain rate for both directions. The symbols represent the atomistic data and the lines were obtained from the previous fits. We see from Fig. 8 that we are in the shear-thinning regime (an increase in the shear rate leads to a decrease in viscosity) and the viscosity along the chains direction (the one important to release stress during a phase transition) is significantly smaller than that in the perpendicular direction. This is somewhat evident by examining the T_p crystal structure and more clear by analyzing the MD trajectories. Figure 9 shows snapshots from our runs for $\dot{\gamma} = 4.0 \times 10^{10}$ both in the parallel (top panels) and perpendicular (bottom panels) directions. While both deformations lead to disorder of the chains, the perpendicular case involves much larger molecular rotations and relative shifts, and consequently larger energies and stresses.

VI. CONCLUSIONS

We used a combination of *ab initio* (DFT-GGA) calculations and MD with first principles force fields to characterize several "unit mechanisms" that govern the electromechanical properties of electroactive polymers PVDF and P(VDF-TrFE) (50-50). The quantum mechanics calculations of energetics and structures of various phases of PVDF and P(VDF-TrFE) show that T configurations are stabilized energetically by the addition of bulkier F atoms in TrFE. This result is
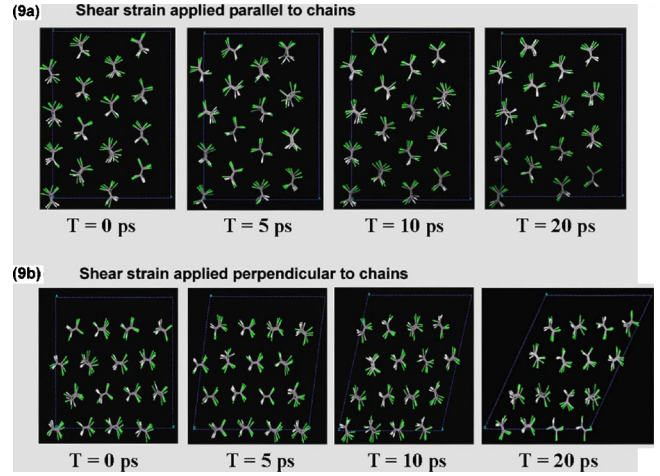
likely related with the better crystallinity and piezoelectric properties of P(VDF-TrFE), because of its stabilization of the all-T from T_p. Our results also show that conformations with T and G bonds are energetically favorable for large interchain separations as compared with all-T structures; this observation is consistent with the experimental observation that samples bombarded with high-energy electrons favor T_3G nonpolar conformations.

Our MD results show that the energy barrier required to nucleate a G bond in an all-T configuration in P(VDF-TrFE) is ~40% lower than in PVDF. Experimentally copolymers show a P-N PT upon heating before melting while PVDF directly melts; this is consistent with the calculated nucleation barriers.

We also studied the motion of the interface separating nonpolar T_3G_{au} and polar T_p phases under uniaxial stress to model the reversible phase transition responsible for electrostriction in electron irradiated P(VDF-TrFE). We found a smaller threshold stress and higher domain wall mobility in P(VDF-TrFE) as compared to PVDF. Interface mobility is an important property for actuators and MD provides a detailed understanding and quantitative characterization of this process that should be useful in mesoscopic or macroscopic simulations. Finally, our simulations of the dynamics of chain sliding reveal that slip occurs more easily along the direction of the chains than perpendicular to them.

In summary we have used first principles-based multiscale modeling to characterize dynamical and static properties PVDF and its copolymers with TrFE. Our simulations are consistent with available experimental observations. In order to make a more quantitative comparison between our dynamical calculations and experiments, we are currently using the atomistic results with mesoscopic modeling[28] to *predict* the behavior of a real actuator whose performance can be directly compared to experiments. We foresee that such multiscale simulations will be an important tool to guide the design of new materials with improved properties.

*Also at: Theoretical Division, Los Alamos National Laboratory, Los Alamos, New Mexico 87545.

†Author to whom correspondence should be addressed. Electronic address: wag@wag.caltech.edu

[1] H. S. Nalwa, *Ferroelectric Polymers: Chemistry, Physics, and Applications* (Marcel Dekker, New York, Basel, Hong Kong, 1995).

[2] T. Furukawa, Phase Transitions **18**, 143 (1989).

[3] Q. M. Zhang, V. Bharti, and X. Zhao, Science **280**, 2101 (1998).

[4] N. Karasawa and W. A. Goddard III, Macromolecules **25**, 7268 (1992).

[5] N. Karasawa and W. A. Goddard III, Macromolecules **28**, 6765 (1995).

[6] G. J. Kavarnos and R. W. Holman, Polymer **35**, 5586 (1994).

[7] R. W. Holman and G. J. Kavarnos, Polymer **37**, 1697 (1996).

[8] G. J. Kavarnos, H. C. Robinson, and R. W. Holman, Ferroelectrics **205**, 133 (1998).

[9] Y. Abe and K. Tashiro, Polymer **42**, 3409 (2001).

[10] Y. Abe and K. Tashiro, J. Polym. Sci., Part B: Polym. Phys. **39**, 689 (2001).

[11] Y. Abe and K. Tashiro, Polymer **42**, 9671 (2001).

[12] A. J. Lovinger, Macromolecules **14**, 322 (1981).

[13] P. A. Schultz, *SeqQuest Electronic Structure Code* (Sandia National Laboratories, 2002).

[14] P. J. Feibelman, Phys. Rev. B **35**, 2626 (1987).

[15] J. P. Perdew, K. Burke, and M. Ernzerhof, Phys. Rev. Lett. **77**, 3865 (1996).

[16] Supplementary Material Available: Force Field File, 2003.

[17] K. Koga and H. Ohigashi, J. Appl. Phys. **59**, 2142 (1986).

[18] Z. Y. Cheng, D. Olson, H. S. Xu, F. Xia, J. S. Hundal, Q. M. Zhang, F. B. Bateman, G. J. Kavarnos, and T. Ramotowski, Macromolecules **35**, 664 (2002).

[19] W. P. Li, Y. W. Tang, S. S. Guo, D. H. Wang, G. Yang, R. H. Wang, and X. Z. Zhao, Appl. Phys. Lett. **82**, 2136 (2003).

[20] H. Dveyaharon, P. L. Taylor, and A. J. Hopfinger, J. Appl. Phys. **51**, 5184 (1980).

[21] N. A. Pertsev and A. G. Zembilgotov, Macromolecules **27**, 6936 (1994).

[22] H. Dvey-Aharon, T. J. Sluckin, and P. L. Taylor, Phys. Rev. B **21**, 3700 (1980).

[23] S. T. Cui, P. T. Cummings, and H. D. Cochran, Mol. Phys. **93**, 117 (1998).

[24] F. Spaepen, Acta Metall. **25**, 407 (1977).

[25] A. S. Argon, Acta Metall. **27**, 47 (1979).

[26] L. Stainier, A. M. Cuitino, and M. Ortiz, J. Mech. Phys. Solids **50**, 1511 (2002).

[27] A. M. Cuitino, L. Stainier, G. F. Wang, A Strachan, T. Cagin, W. A. Goddard, and M. Ortiz, J. Comput.-Aided Mater. Des. **8**, 127 (2002).

[28] A. M. Cuitiño and S. Zheng (unpublished).